Revised Paper ER-19-11586

The Energy Performance Improvement of a PEM Fuel Cell with Various Chaotic Flowing Channels

Pengcheng Dong [1], Yuxin Jia [1]

Gongnan Xie [1,*], Meng Ni [2],

[1] *School of Marine Science and Technology, Northwestern Polytechnical University, P.O. Box 24, Xi'an, 710072, China.*

[2] *Building Energy Re search Group, Department of Building and Real Estate, The Hong Kong Polytechnic University, Hong Kong, PR China.*

[*] Corresponding address: School of Marine Science and Technology, Northwestern Polytechnical University, P.O. Box 24, Xi'an, 710072, China. Tel: +86-29-88492611; Fax: +86-29-88495278. E-mails: xgn@nwpu.edu.cn (G. Xie).

The Energy Performance Improvement of a PEM Fuel Cell with Various Chaotic Flowing Channels

P. C. Dong, Y. X. Jia, G. N. Xie, M. Ni

Abstract: *To improve the energy performance of a Proton Exchange Membrane Fuel Cell (PEMFC), novel chaotic structures are proposed and numerically evaluated for replacing straight types in the serpentine gas diffusion flow channels. The numerical model is verified by the available experimental data. Nine cases (chaotic channels, Cases A2, B1, B2, C1, C2, D1, D2, E1 and E2) and a baseline case (straight flow channel, Case A1) are evaluated, and the detailed temperature and the flow characteristics are presented and analyzed. The influences of the main design parameters including the corner angle, bends number and datum surface number are also analyzed and concluded. It is found that the newly proposed chaotic structures can improve not only the temperature uniformity but also the maximum output power and the energy efficiency of the PEMFC. Compared with a traditional PEMFC, the power output of the new PEMFCs with chaotic flowing channels can be improved by 6.26% and the efficiency of PEMFC can be promoted by 8.40%.*

Keywords: *PEMFC; Chaotic geometry; Temperature uniformity; Pressure drop; Current-power curves; Energy efficiency.*

Nomenclature

a_{H_2O} = water activity

A = area (m^2)

AR = aspect ratio

c_p = specific heat capacity ($J \cdot kg^{-1} \cdot K^{-1}$)

C = molar concentration ($kmol \cdot m^{-3}$)

C_B = total reactants concentration

D = diffusion coefficient ($m^2 \cdot s^{-1}$)

D = diameter (m)

E = voltage (V)

f = friction factor

F = Faraday constant, 96485 $C \cdot mol^{-1}$

h = heat (J)

H = height (m)

i = current density ($A \cdot m^{-2}$)

i_0 = exchange current density ($A \cdot m^{-2}$)

i_L = limiting current density ($A \cdot m^{-2}$)

I = current (A)

J = transfer current density ($A \cdot m^{-3}$)

k = thermal conductivity ($W \cdot m^{-1} \cdot K^{-1}$)

K = impedance

L = length (m)

m = flow channel datum surface number

M = molecular weight ($kg \cdot kmol^{-1}$)

$M_{m,dry}$ = equivalent weight of a dry membrane ($kg \cdot kmol^{-1}$)

MD = mean deviation

n = flow channel bends number

n = electron transfer number

n_d = electro-osmotic drag coefficient

N = sample number

P = pressure (kPa)

P = power (W)

R = Universal gas constant, 8.314 $kJ \cdot kmol^{-1} \cdot K^{-1}$

S = source term in governing equations

T = temperature (K)

u = velocity ($m \cdot s^{-1}$)

V = potential (V)

W = width (m)

x = coordinate of the fluid flow direction

X = mole fraction

y = coordinate of the width direction

Y = mass fraction

z = coordinate of the height direction

Greek symbols

α = angle of flow channel corner

α = charge transfer coefficient

δ = diffusion distance (m)

ε = porosity

η = over-potential (V)

λ = water content

μ = viscosity ($kg \cdot m^{-1} \cdot s^{-1}$)

ρ = density ($kg \cdot m^{-3}$)

$\rho_{m,dry}$ = density of dry membrane ($kg \cdot m^{-3}$)

σ = electrical conductivity ($\Omega \cdot m^{-1}$)

σ = standard deviation

ϕ = phase potential (V)

Subscripts

act = active region

an = anode

ca = cathode

cd = computational domain

ch = flow channel

cl = catalytic layer

d = distance

dl = diffusion layer

eff = effective

f = fluid

H = hydraulic

H_2 = hydrogen

H_2O = water

i = gas species

L = local

mix = mixture

ohm = resistivity

O_2 = oxygen

p = flow field plate

pem = proton exchange membrane

r = rise

$react$ = reaction

ref = reference

sat = saturate

sol = solid phase

1. Introduction

Environmental pollution and the fossil fuel depletion requires more efficient energy conversion technologies. Due to the advantages of high efficiency, high power density, low (or zero) pollutant emission, fuel flexibility, and quiet operation, fuel cell is a very promising electrochemical energy conversion device [1]. PEMFC is the most promising fuel cell for fuel cell vehicles and for residential and portable power applications [2].

The operating temperature of PEMFC plays a significant role in PEMFC performance. The proton conductivity of the electrolyte membrane and the activity of the catalyst is highly dependent on the temperature. The operating temperature of low-temperature PEMFCs should be controlled 60 to 70 °C, while the working temperature of high-temperature PEMFCs is about 100 to 200 °C [3]. Higher temperatures can increase the rate of electrochemical reaction and diffusion [4]. The structural design of a PEMFC play an important role in its temperature distribution. A good flow channels design is critical to improve the durability of a PEMFC.

Various research works have focused on the design of the flow channels. Common designs of PEMFC flow channels include parallel flow channel [5], serpentine flow channel [6], spiral flow channel [7], grid flow channel [8], intersectant flow channel [9], fractal flow channel [10] and so on. Also some other designs of flow channels such as install baffle plates into flow channel [11] or add blocks into flow channels [12]. From the literature, it is found that there are both pros and cons of each form of flow channels. In Ref. [13], developments of PEMFCs mathematical modeling were presented and summarized. The effects of temperature, pressure, humidity on transport characteristics were discussed with their effects on the fuel cell performance [14,15]. Yin et al. [16] established a three-dimensional model with the installation of baffle plates. They found that the sloping angles and the baffle plate number could change the output performance of fuel cell. The effect of the opening size of the cathode outlet on the performance of PEMFC was studied through the experiment by Chen et al. [17]. A porous-

blocked baffled flow channel proposed and its contribution to the performance of PEMFC studied [18]. In order to better evaluate the performance of PEMFC, a new evaluation criteria and cathode flow channel are proposed in Ref. [19].

Recent studies have shown that in flow channels of special geometries, the diffusion characteristics of laminar flow can be close to that of turbulent flow. This phenomenon is called chaotic advection (or Lagrangian turbulence, Lagrangian chaos). Under this flow state, two-phase flow is produced and the particle trajectory of the fluid is shown as a chaotic state which can increase the mixing between the fluid and promote the heat exchange between the cold fluid and the heat transfer wall in the middle of the flow channel. Therefore, the heat transfer is enhanced and the pressure drop is not increased significantly [20,21].

As a new heat transfer enhancement technology, chaotic convection has received increasing attention in recent years. The research of the three-dimensional chaotic twisted geometry was mainly concentrated on heat transfer by Babiraei et al. [22]. It was concluded that the Lagrangian dynamics quickly evolves into a complicated flow pattern because of small-scale structural changes. In Ref. [23,24], the hydrothermal features and temperature uniformity of C-shaped channel are studied at low Reynolds. The phenomenon of heat transfer enhancement in a helical tube was analyzed by Lemenand and Peerhossaini [25] and Acharya et al. [26]. Castelain et al. [27] studied the effect of simple chaotic channel on the performance of PEM fuel cell through experiments. Xuan et al. [28] utilized a CFD/electrochemical model to estimate the efficacy of the mechanism underlying a chaotic flow-based fuel cell.

Based on the articles mentioned above about chaotic flow channels [19-28], the heat and mass transfer statuses are changed because of Lagrange chaos produced due to chaotic structures in flow channels. As the temperature uniformity and output performance of PEMFCs can be affected largely by the heat and mass transfer inside, the chaotic structures could be effective in

improving the performance of PEMFC. However, no numerical study has been conducted to evaluate the effects of chaotic structure on PEMFC performance.

To fill in the research gap, nine different shape of chaotic flow channels which are all composed of a succession of curved and straight segments are designed and investigated numerically for their application in PEMFC. The flow channels of four cases have only one datum surface and the other five cases have two different datum surfaces. They are also set with different flow channel corner angles and bends amount. In this research, the performance of PEMFCs using these nine chaotic flow channels are compared with the one with straight flow channel. The influence of datum surface number (m), bends number (n) and corner angle (α) are compared and analyzed. Based on the conclusions which are drawn in this paper, some deeper researches can be conducted in the future.

2. Description of Physical Models

In this paper, the PEMFC with serpentine flow channels is chosen due to its wide use in fuel cells. Take Case A1 as an example, Fig. 1 shows the diagram of a PEMFC with serpentine flow channels. A sketch of 3D integrated system is shown in Fig. 1 (a). A PEMFC consists of current collectors, diffusion layers, catalyst layers and membrane. As the performance of PEMFC can be improved using counter flow, hydrogen and air are injected into the flow channels of anode and cathode from different ends of the flow channels respectively. The aspect ratio (AR) of the flow channels *is* 1:2 with the width and height of the flow channel cross section are W_{ch}= 2 *mm*, H_{ch}= 1 *mm* respectively. As for the other design parameters, the height of the flow field plate H_p= 2 *mm*, the height of diffusion layer is equal to that of the proton exchange membrane H_{dl}= H_{pem}= 0.05 *mm*, the height of catalyst layer H_{cl}= 0.2 *mm*, as shown in Fig. 1 (b). In Fig. 1 (c), the representative line and surfaces for are given. Line 1 is the center-line of the anode flow channel. Sur 1 is the mid surface in z axis direction of membrane (z= 0 *mm*). Sur 2 and Sur 3 are the mid surface in z direction of anode flow channel in cases 1 and cases 2,

respectively. Sur 4, Sur 5 and Sur 6 are three critical streamwise-normal planes whose coordinates are x= 3 *mm*, x= 11 *mm* and x= 15 *mm*.

In this study, the work is devoted to the designs of the 3D geometries that can produce chaotic advection. Nine kinds of chaotic flow channels benefiting from chaotic advection without introducing large 3D geometries are considered under the comparison of straight flow channel (Case A1). These parameters of model developing are listed in Table 1 for the convenience of readers. The cases are designed with different values of flow channel datum surface number (m), flow channel bends number (n) and flow channel corner angle (α). And these values of cases are listed in Table 2. For the cases whose m= 2, the height rise between different datum surfaces H_r= 0.5 *mm*. As the design of the flow channels are repeated in x direction, in this study, the computational domains are limited to one basic design called a period to reduce the computational load. The flow channels of one period are all designed as the succession of straight and curved segments as shown in Fig. 2. A multiplicity of designs is possible based on these alternatives. The three-dimensional computational domain of the PEMFC used in this research includes flow field plates, flow channels, diffusion layers and catalyst layers in the anode and cathode and proton exchange membrane in the middle. To control the variables, for all flow channels investigated in this paper, the width, length and height of the computational domain for these ten cases are the same, W_{cd}= 14 *mm*, L_{cd}= 18 *mm* and H_{cd}= 4.55 *mm*. Also, the width of flow channel interval is the same, W_{in}= 2 *mm*.

3. Computational Details

3.1 Overview

In this study, the temperature field and flow field analysis in PEMFCs with chaotic flow channels are mainly carried out with the commercial software FLUENT version 14.5. The finite volume method is used to solve the fluid flow and heat transfer governing equations with suitable boundary conditions. The mesh is generated by the software ICEM CFD version 14.5.

3.2 Assumptions

As a PEMFC system has very high complexity, it is necessary to make the following basic assumptions under condition that the simulated results are not influenced when a PEMFC system is established and simulated:

- All gas components involved in this research are ideal gases in-compressible;
- Gas flow in PEMFCs can be regarded as laminar flow, as gas flow rates are low and flow channel cross-sectional area is small thus the Reynolds number is low.
- All porous material which refers to gas diffusion layer, catalyst layer and proton exchange membrane in PEMFC simulation are isotropic and homogeneous;
- Forced convection heat transfer effect is applied to the cooling of PEMFC system.
- The electrochemical kinetics are described by the Butler-Volmer equation.

3.3 Governing equations

At the anode side of a PEMFC, hydrogen molecules flow through the flow channel, penetrate into the diffusion layer, and oxidize to yield protons and electrons (Eq. 1). The protons are then transported to the cathode side through the membrane. The electrons cannot go through the membrane while are transported to the cathode side through an external circuit. At the cathode side, oxygen molecules which are injected in the PEMFC system from cathode flow channel, pass through the diffusion layer, and reach the catalyst layer where the reaction of oxygen molecules and protons (Eq. 2) take place. All in all, the overall reaction occurring in a PEMFC is shown in the Eq. (3). Part of chemical energy in fuel and oxidant is converted to electrical power and the other is wasted as heat [29].

$$H_2 \rightarrow 2H^+ + 2e^- \tag{1}$$

$$\frac{1}{2}O_2 + 2H^+ + 2e^- \rightarrow H_2O \tag{2}$$

$$H_2 + \frac{1}{2}O_2 \rightarrow H_2O \tag{3}$$

In this study, a PEMFC is simulated by a 3D, non-isothermal, single-phase and steady state model. Following are governing equations of physical and electrochemical phenomena that take place inside a PEMFC.

Mass Conservation [30-33]:

Eq. (4) is the continuity equation where the calculate method of mixture density is provided in Eq. (5). The source terms for the consumption of hydrogen, oxygen and the creation of water can be calculated by Eqs. (6), (7) and (8), respectively.

$$\nabla \cdot (\rho \vec{u}) = S_{\mathrm{H}_2} + S_{O_2} + S_{H_2O} \tag{4}$$

$$\rho_{mix} = \frac{P}{RT\sum \frac{Y_i}{M_i}} \tag{5}$$

$$S_{H_2} = -\frac{J_{an}}{2F} M_{H_2} \tag{6}$$

$$S_{O_2} = -\frac{J_{ca}}{4F} M_{O_2} \tag{7}$$

$$S_{H_2O} = +\frac{J_{ca}}{2F} M_{H_2O} \tag{8}$$

According to the Butler-Volmer equation, the volumetric transfer current densities can be determined at the anode and cathode sided as follows.

$$J_{an} = \xi_{an} j_{an}^{ref} (\frac{C_{H_2}}{C_{H_2}^{ref}})^{\gamma_{an}} (\exp(\frac{\alpha_{an} F}{RT} \eta_{an}) - \exp(\frac{-\alpha_{ca} F}{RT} \eta_{an})) \tag{9}$$

$$J_{ca} = \xi_{ca} j_{ca}^{ref} (\frac{C_{O_2}}{C_{O_2}^{ref}})^{\gamma_{ca}} (-\exp(\frac{\alpha_{ca} F}{RT} \eta_{ca}) + \exp(\frac{-\alpha_{ca} F}{RT} \eta_{ca})) \tag{10}$$

The over-potential at the anode or cathode side is calculated by

$$\eta = \phi_{sol} - \phi_{pem} - V_{ref} \tag{11}$$

where V_{ref} is the reference voltage. At anode and cathode sides, it is set as 0 and negative open circuit voltage (OCV) respectively.

Species transport [30,31 and 34]:

The species transport equation is

$$\nabla \cdot (\rho \vec{u} Y_i) = \nabla \cdot (\rho D_i^{eff} \nabla Y_i) + S_i \tag{12}$$

where D_i^{eff} is the effective gas species and can be approximated by using Eq. (13), which can only be used in the catalyst layers.

$$D_i^{eff} = \varepsilon^{1.5} D_i \tag{13}$$

Phase potential [33,35]:

The second important driving force in a PEMFC is surface over-potential which represents the difference between the phase potentials of the electron conductor and proton conductor. The phase potential equations for these two kinds of conductors are shown in Eqs. (14) and (15), respectively.

$$\nabla \cdot (\sigma_{sol} \cdot \nabla \phi_{sol}) + S_{sol} = 0 \tag{14}$$

$$\nabla \cdot (\sigma_{pem} \cdot \nabla \phi_{pem}) + S_{pem} = 0 \tag{15}$$

The ionic conductivity of the membrane is determined by the water content and temperature, as shown in Eq. (16). The relations between the source terms of phase potential equations and the transfer current densities are shown in Eqs. (17) and (18) respectively.

$$\sigma_{pem} = (0.514\lambda - 0.326)\exp(1268(\frac{1}{303} - \frac{1}{T})) \tag{16}$$

$$S_{\text{sol}} = -j_{an,ca} \tag{17}$$

$$S_{\text{pem}} = j_{an,ca} \tag{18}$$

Energy [30]:

The energy equation in a PEMFC is

$$\nabla \cdot (\rho c_p \vec{u} T) = \nabla \cdot (k \nabla T) + S_{\text{h}} \tag{19}$$

where S_{h} is the source term in Eq. (19), and can be calculated by

$$S_{\text{h}} = I^2 R_{ohm} + h_{react} - j_{an,ca} \eta_{an,ca} \tag{20}$$

Momentum [30,32]:

The momentum equation is

$$\nabla \cdot \left(\varepsilon \rho \vec{u}\vec{u} \right) = -\varepsilon \nabla p + \left(\nabla \cdot \varepsilon \mu \vec{u} \right) + S_u \tag{21}$$

where S_u is the source term, which is useful in the diffusion layer and catalyst layer, and is defined by.

$$S_u = -\frac{\mu}{k_p} \varepsilon \vec{u} \tag{22}$$

Water transport through the membrane [36,37]:

There are three causes of water transport through the membrane. These causes are electro-osmotic drag, water concentration gradient, and pressure gradient which is omitted in this paper. The governing equations of these phenomena is

$$\nabla \cdot (\frac{n_d \cdot M_{H_2O}}{F} \vec{I} - D_{H_2O} \nabla C_{H_2O}) = 0 \tag{23}$$

where n_d, D_{H_2O} *and* C_{H_2O} are electro-osmotic drag coefficient, water diffusivity, and water mass concentration and can be calculated by

$$n_d = 2.5 \frac{\lambda}{22} \tag{24}$$

$$D_{H_2O} = \begin{cases} 3.1 \times 10^{-7} \lambda (\exp(0.28\lambda) - 1) \exp(-\frac{2346}{T}) & \lambda \le 3 \\ 4.17 \times 10^{-8} \lambda (1 + 161 \exp(-\lambda)) \exp(-\frac{2346}{T}) & \lambda > 3 \end{cases} \tag{25}$$

$$C_{H_2O} = \frac{\rho_{m,dry}}{M_{m,dry}} \lambda \tag{26}$$

where λ is membrane water content and can be calculated as:

$$\lambda = \begin{cases} 0.043 + 17.81 a_{H_2O} - 39.85 a_{H_2O}^2 + 36 a_{H_2O}^3 & 0 < a_{H_2O} \le 1 \\ 14 + 1.4 (a_{H_2O} - 1) & 1 \le a_{H_2O} \le 3 \end{cases} \tag{27}$$

where a_{H_2O} is water activity and can be obtained by Eq. (28).

$$a_{H_2O} = \frac{X_{H_2O} P}{P_{sat}} \tag{28}$$

Based on the governing equations mentioned above, the expressions of quantities which are used in the analysis of results are as follows.

Polarization curve [38]:

Due to the slow speed of the oxidation-reduction reaction, most of the voltage losses occur in the cathode. Therefore, the voltage losses in the anode are ignored, and the voltage of a single PEMFC can get a sufficiently accurate approximation as

$$V = E - \frac{RT}{\alpha F}\ln(\frac{i}{i_0}) - \frac{RT}{nF}\ln(\frac{i_L}{i_L - i}) - iR \tag{29}$$

the limiting current density, according to the Fick's law, is $i_L=nFDC_B/\delta$, where C_B is total reactants concentration.

As power is defined as the product of potential and current, it can be expressed as:

$$P = ViA_{act} \tag{30}$$

where A is the area of active region of PEMFCs.

Pressure drop [38]:

Considering the flow channel designs in this research, the pressure drop of flow channel is the same as that of whole flow field. Therefore, the pressure drop can be approximated using uncompressed liquid equations in tubes when the pressure drop is smaller than 30% of the inlet. Thus it can be determined by the following equations with enough accuracy:

$$\Delta P = f\frac{L_{ch}}{D_H}\rho_f\frac{\bar{u}^2}{2} + \sum K_L\rho_f\frac{\bar{u}^2}{2} \tag{31}$$

where K_L is local impedance (e.g. where has sudden turning), D_H is hydraulic diameter of flow channel and $D_H=2W_{ch}H_{ch}/(W_{ch}+H_{ch})$.

Efficiency [38]:

The efficiency of PEMFC is directly proportional to the potential. When we use the high heat value of hydrogen (i.e. ΔH= 286 *kJ/mol*), η= V/1.482. But more often (also in this paper),

the low heat value of hydrogen (i.e. ΔH= 241 *kJ/mol*) is used, the efficiency of PEMFC can be calculated by

$$\eta = \frac{V}{1.254} \tag{32}$$

3.4 Boundary conditions

Based on above-mentioned assumptions, the boundary potential at anode is assigned to be zero and the output voltage at cathode is set to be boundary potential. Mass flow inlet $m_{in} = \int_A \rho \vec{u} \cdot \vec{n} dA$ and pressure outlet are applied at the inlet and outlet, respectively. The pressure of the outlets is set to be the standard atmospheric pressure. No slip conditions are applied to fixed walls. Other key operating parameters and their values applied in the present simulations of all computational models are listed in Table 3.

3.5 Grid independence

The mesh used in this study is made by ICEM CFD software. The mesh near the flow channels are shown in Fig. 3(take Case E1 as an example). Case A1 is taken as an example to check the grid independence. Three different meshes with 3.42 million elements, 4.69 million elements and 5.67 million elements are tested with the same boundary conditions. Fig. 4 plots a comparison of the streamwise velocity along the centerline of anode flow channel for Case A1 under the three mesh systems. It can be seen that the velocity results under mesh systems with 4.69 million elements and 5.67 million elements are similar to each other, while the result under the mesh system of 3.42 million elements is different from the other two, especially at the beginning part. Considering the balance between computational economy and simulated accuracy, the mesh system with 4.69 million elements is used for Case A1 in this numerical simulation. Similar, the elements number of mesh systems for other nine cases are between 4.61 million and 4.80 million.

3.6 Model validation

One proper selection of the simulation model is very important as it can influence the accuracy of the results to a great extent. Therefore, a model validation was implemented by comparing with experimental data from Wang et al. [39] as shown in Fig. 5. The operating temperature and pressure are set to be the same with the experimental conditions that are 343 *K* and 1atm, respectively. It was found that the polarization curve of numerical results agree with the experimental data from Ref. [39]. So, the fuel cell and electrolysis model has been selected for all cases and the model used in this simulation work is sufficiently accurate.

4. Results and Discussion

4.1 Temperature fields

The temperature fields of PEMFCs with nine different chaotic cases are compared with that of the straight flow channel (Case A1). The model parameters for the ten cases are the same as mentioned above. The overhead view of the cases in the same line are the same, only the flow channel datum surface numbers of cases 2 equal to 2 while those of cases 1 equal to 1. For cases B and cases D, the flow channel corners are right angles (α= 90°), and α= 45° for cases C and cases E. The bend amount of cases B and C are the same (n= 10), meanwhile, that of cases D and E are the same and more than cases B and C (n= 14).

The performance of the membrane is affected significantly by the temperature, however, excessively high temperature may cause a PEMFC not work properly and low temperature would lead to slow electrochemical reaction, the temperature of the membrane mid surface (z= 0 *mm*) is extremely important. The temperature distributions of all these ten cases on this surface are chose to be compared and analyzed as shown in Fig. 6. The highest temperatures of all these ten cases included the case with straight flow channel are near the inlets, because the fuel and air injected in flow channels is much hotter compared with the operation temperature of the PEMFC. Besides, the temperature near the flow channels is higher than the farer area until the temperature

of fuel and air decrease to be the operating temperature because the high temperature fuel and air flows along the flow channel.

In Fig. 6, the cases in the left column are PEMFCs whose flow channels only have one datum surface (cases A1, B1, C1, D1, and E1) and the cases in the right column are cases whose flow channels have two datum surfaces at different heights (cases A2, B2, C2, D2, and E2). The temperatures of the right column cases are significantly lower in the middle part of the whole PEMFC. As the flow channels of these cases are at different datum surfaces, the middle part of them are higher than the other parts. Therefore, the temperature of these parts is lower than the same area of the cases whose flow channels are at the same level because of the heat loss and the decreased reactant concentration in the process of heat transfer.

With different flow channel corners, the temperature uniformity of the cases whose α= 45° are better than the cases whose α= 90°. The reason is that there are more significantly dead zones for cases B and D (α= 90°) which impede the fully mix of fluid. As for temperature distributions of the cases whose only difference is the amount of flow channel bends, the difference of the temperature distributions between each other are slight and cannot be seen clearly in the temperature field isopleths. Therefore, some more analysis about the uniformity of the membrane mid surface temperature are carried out in the following part.

4.2 Temperature uniformity

As the judgment of temperature uniformity on the membrane mid surface cannot be made directly from the temperature nephogram, to find out whether the temperature uniformity of cases with chaotic structure flow channels are better, one or more quantities need to be set to characterize the temperature uniformity. Therefore, we define two quantities: mean deviation (*MD*) and standard deviation (σ) to express the degree of temperature uniformity.

4.2.1 Mean deviations

The temperature mean deviations of different cases on the mid surface of membrane (z= 0 *mm*) are calculated and compared in this part. To ensure fair comparisons, 1000 points are chosen randomly in each case. We collected the temperature of these points and used them to calculate the mean deviation and standard deviation to analyze the temperature uniformity of the membrane mid surface. The mean deviation is defined as

$$MD = \frac{\Sigma \left| T - \bar{T} \right|}{N} \tag{33}$$

In Fig. 7 (a), the mean deviations of membrane mid surface temperature are shown. It can be clearly seen that the mean deviations of cases 1 are larger than that of cases 2. Therefore, the temperature uniformity of the membrane mid surface temperature in cases whose flow channels have two datum surfaces at different height is better than that in cases whose flow channels have only one datum surface significantly. For cases B and D whose angle of the flow channel corners α are both equal to 90°, but the amounts of the flow channel bends n of cases D are larger than that of cases B, the mean deviations of cases D are larger than that of the corresponding cases B. As for cases C and E (α= 45°), the principle is the same, that is, the mean deviations of cases E (whose n is larger) are larger than that of the corresponding cases C. Therefore, decreasing the amount of flow channel bends n is propitious to enhance the uniformity of the membrane mid surface temperature no matter the flow channels of the cases are at the same or different levels. However, when it comes to the comparison of the cases with different flow channel corners' angles α, the principle of cases whose flow channels have only one datum surface (cases 1) is different from the principle of cases whose flow channels have two different datum surfaces (cases 2). For cases 1, the mean deviations of cases B1 and D1 are larger than that of cases C1 and E1. Meanwhile, the mean deviation of Case A1 is smaller than all mean deviations of the other cases. So, it can be concluded that when the flow channel of a PEMFC has only one datum surface, the straight serpentine flow channel performs best in the uniformity of membrane mid surface temperature, flow channels whose corners' angles equal to 45° take the second place, and

flow channels whose corners' angles equal to 90° give the worst performance. For cases 2, this principle is so different from that of cases 1, and the differences between the mean deviations of cases 2 are much smaller than that in cases 1. The mean deviation values of cases A2 and C2 are nearly the same and slightly smaller than that of Case E2. However, cases B2 and D2 have the smallest mean deviation values. So, the conclusion that when the flow channels of the PEMFC have two different datum surfaces, cases with flow channel corners' angle equal to 90° have the best temperature uniformity can be drawn.

4.2.2 Standard deviations

The same as in part 4.2.1, in each of the ten cases, we randomly chose 1000 points on the mid surface of membrane, collected the temperature of these points and carried out the calculation of the standard deviation of these temperatures. The comparison of the standard deviations which defined as

$$\sigma = \sqrt{\frac{1}{N}\sum(T - \bar{T})^2} \tag{30}$$

of the ten cases are shown in Fig. 7 (b). The general trend of the standard deviations in Fig. 7 (b) is the same with that of the mean deviations in Fig. 7 (a) which confirm the principles we induced in part 4.2.1. The only difference is that the standard deviation of Case C2 is significantly larger than that of Case A2 while the mean deviations of cases C1 and A1 are nearly the same. All in all, the cases whose flow channels have two different datum surfaces and the cases whose flow channel bends number is small have better performances on membrane mid surface temperature uniformity. The influence of flow channel corner angles on temperature uniformity depends on whether the flow channels have only one datum surface or more.

4.3 Velocity distributions

To find out the specific flow situation in the PEMFC, the velocity distributions of the mid surface of anode flow channels in these ten cases under the same conditions are shown in Fig. 8. The configuration of the cases is the same as in Fig. 6. There are all dead zones at the flow

channel corners in all these ten cases, but the area and location of the dead zones vary in different cases.

From Fig. 7, it can be seen that the velocity increment in cases A is not so significant as the other eight cases because of the lack of vortexes produced due to the chaotic structure in the flow channels of the other cases. The high velocity region in cases 1 (left column) is larger than that in cases 2 (right column). This is because the resistance effect of the chaotic structure in the *z* axis direction. Meanwhile, the locations of the dead zones in cases which are in the same line (e.g. Case A1 and Case A2) are similar to each other. But the dead zone area in cases whose flow channels have two different datum surfaces (e.g. Case A2) are obviously much smaller than the corresponding case whose flow channel has only one datum surface (e.g. Case A1). However, the general velocity distribution trend are the same in cases in the same line.

When comparing the cases with different flow channel corner angles (α) and the same the other design parameters (e.g. Case B1 and Case C1), the dead zone area in cases with the flow channel corner angles α equal to 90° (e.g. Case B1) is much larger than that in cases whose α equal to 45° (e.g. Case C1), however, the velocity increasing effect of cases whose α equal to 90° is also more significant. When the comparison comes to the cases with different amount of flow channel bends (n) and the same the other design parameters (e.g. Case B1 and Case D1), the difference between the dead zones is not significant. However, the cases with smaller flow channel bends amount (e.g. Case B1) have more obvious velocity increasing effect. Therefore, cases with larger flow channel angles and smaller flow channel bends amount have more violent velocity increasing effect. And the influence of flow channel corner angles on the location and area of dead zone is much more obviously than the influence of flow channel bends amount.

4.4 Streamlines

The flow streamlines shown in Fig. 9 and Fig. 10 are presented for streamwise normal planes Sur 4, Sur 5 and Sur 6 to illustrate how fluid flows at critical planes.

In Fig. 9, flow streamlines of cases with different *m* (take cases A1 and A2, B1 and B2 as examples) are shown and compared. In Cases A1, Sur 4 and Sur 6 are streamwise normal planes where flow channels take a turn and Sur 5 is a streamwise normal plane in process of straight part in the flow channel which is set to compared with the other cases. In Case A2, there are all changes of flow channel datum surfaces in all these three surfaces. In both cases A1 and A2, the vortices are generated more significantly in the middle part of a PEMFC as shown in Sur 5. However, more vortices are observed in cathode flow channel as the inlet velocity of fluid in cathode is larger than that in anode flow channel. Comparing cases A1 and A2, it is easier for Case A2 to produce vortices because of the changing of flow channel datum surface change in flow channels. When the comparison comes to cases B1 and B2, this difference becomes much greater especially at Sur 4 and Sur 5 which are the middle surfaces of the flow channel bends in streamwise direction. At these two surfaces of Case B2, there are distinct vortices near the walls of flow channels. Also, the flow streamlines at Sur 4, Sur 5 and Sur6 of cases with different *n* (take cases B1 and D1, C1 and E1 as examples and compared with Case A1) and α (cases B1 and C1, D1 and E1 are taken as examples while Case A1 is set as a reference) are shown and compared in Fig. 10. In this figure, one can find that there is no fixed flow law in cases with chaotic structure flow channels. This situation is caused by the chaotic structure of flow channels which can produce Lagrange chaos in fluid.

4.5 Output power

As PEMFCs are used to produce electric energy, a very important evaluation criterion of the PEMFCs is the output power which is compared in this part. The current-power curves of typical cases with different flow channel datum surface numbers (*m*), bends numbers (*n*) or bends angles (α) are plotted and compared in Fig. 11. Among these figures, Fig. 11 (a) and (b) show comparisons of cases with different *m*, Fig. 11 (c) and (d) compare cases with different *n*, and the comparison of different α cases are shown in Fig. 11 (e) and (f).

When comparing cases with different *m*, the output power in cases A2 and B2 is larger than that in cases A1 and B1 under the same current as shown in Fig. 11 (a) and (b). The output power difference in Fig. 11 (a) is much larger than that in Fig. 11 (b). This phenomenon is because that Case A1 is straight serpentine flow channel and cases A2, B1 and B2 are all chaotic structure flow channels. Therefore, although these two figures are all comparisons between two cases whose only difference is the value of m, the difference between cases A1 and A2 is larger than that between cases B1 and B2. However, the conclusion is that cases whose *m* is larger have larger output power no matter what the value of current is. When we compare cases with different *n*, we choose two sets (cases A1, B1 and D1 as shown in Fig. 11 (c) and cases A2, B2 and D2 as shown in Fig. 11 (d)) with different *m* to find out the influence of different flow channel structure (straight flow channel and chaotic structure flow channel). In the comparison of cases A1, B1 and D1, Case B1 whose *n* equal to 10 shows the largest output power under all current values. As for cases A1 and D1, the difference between these two cases in output power is small. However, the output power of Case D1 is larger than that of Case A1 when current is small, and when current is larger than 0.73 A/cm^2, Case A1 gives a larger output power. As for the comparison in Fig. 11 (d), Case B2 gives the largest output power, Case A2 takes the second place, and Case D2 performs the worst. This means that chaotic structure with small flow channel bends number is benefit to output power of a PEMFC, but as *n* increases, this advantage may lose. At last, the influence of α is analyzed using the comparison of cases A1, B1 and C1 in Fig. 11 (e) and cases A1, D1 and E1 in Fig. 11 (f). In Fig. 11 (e), the output power of Case B1 and C1 is nearly the same and larger than that of Case A1. As for in Fig. 11 (f), Case E1 gives a larger output power compared with the nearly the same output power value in cases A1 and D1.

As the maximum output power is a crucial physical quantity that can judge the output performance to a certain extent, this value of all cases is shown in Fig. 12. In this figure, Case D2 gives the smallest value in the maximum output power values which is 8.30 *W*. As the other

cases are all PEMFCs with chaotic structure flow channels, a conclusion can be drawn that chaotic structure is beneficial for the output power of PEMFCs. As the largest output power of chaotic structure cases is 8.83 W (Case B2), the maximum output power is increased by 6.26%. Generally, the maximum output powers of cases 2 are larger than that of the corresponding cases (cases 1) with promote ratios between 0% and 3.21%. Therefore, increasing the datum surface number of the PEMFC flow channels is conductive to improving the output power of PEMFCs. For the cases whose only difference is the flow channel corner angle α (e.g. Case B1 and Case C1), the maximum output powers of cases whose flow channel corner angle α equal to 45° are smaller than that of cases whose flow channel corner angle α equal to 90°. When comparing the cases with different amount of the flow channel bends (e.g. Case B1 and Case D1), cases having smaller flow channel bends perform better in the maximum output power compared with cases having more channel bends. So, we can get a summary that the effects of flow channel datum surfaces, flow channel corner angle and flow channel bends is different. However, increasing the datum surface number are benefit to the maximum output power for PEMFCs with chaotic structure flow channels.

4.5 Pressure drop of the anode flow channel

It is a fact the pressure drop has much influence on the energy consumption of PEMFCs, and for the designs used in this research, the pressure drop of the anode channel is equal to the pressure drop of the whole flow field, the pressure drops of different cases of the anode flow channel are contrasted in this section as shown in Fig. 13. From the table, one can find that Case A1 gives the smallest pressure drop due to its simplest flow channel structure. For cases in the same line, the pressure drop value of case 2 show a difference of about 2 kPa larger than that of the corresponding case 1. The reason of this situation is the impediment to fluid flow on z axis direction caused by the middle lifting flow channel structure.

For cases with different flow channel bends number *n* (e.g. Case B1 and D1), smaller the *n* is, smaller the impediment to fluid flow on *x* axis direction is and therefore smaller the pressure drop of the anode flow channel is. The pressure drop gaps between two cases whose only difference is the flow channel bend number *n* are between a region of 1.46 *kPa* to 3.41 *kPa*. When comparing the cases with different α (e.g. Case B1 whose α equal to 90° and Case C1 whose α equal to 45°), as the structure of flow channel bends with 45° corner angle is much easier to pass by for fluid compared with that of flow channel bends with 90° corner angle, the pressure drop of cases whose α equal to 45° is much smaller than that of cases whose α equal to 90° and the difference is between 7.56 *kPa* to 9.72 *kPa*.

Based on the analysis above, the flow channel corner angle α has quite obvious influence on the pressure drop while the effect of flow channel datum surface number *m* and the flow channel number *n* on the pressure drop is much smaller.

4.6 Efficiency

The efficiencies of all the ten cases including 9 cases with chaotic structure flow channels and a reference case (Case A1) with straight serpentine flow channels are shown in Fig. 14. From the figure, one can find that Case A1 shows the smallest efficiency (41.92%) compared with the other cases which means that chaotic structure flow channels are benefit to the efficiency of PEMFCs. The largest efficiency of chaotic structure cases is 45.44% (Case B2). Chaotic structure flow channels increase the efficiency of a PEMFC by 8.40% comparing with straight serpentine flow channels. Comparing the two cases whose overhead views are the same and the only difference is the flow channel datum surface number *m*, cases 2 have a better performance compared with the corresponding case 1. In cases A, B, C, D and E, the larger efficiencies are 44.18% (Case A1), 45.44% (Case B1), 44.93% (Case C1), 42.19% (Case D1) and 44.37% (Case E1), respectively. With different *n* and α, the promote ratio is between 0.19% and 5.39%. Therefore, increasing the datum surface number *m* of the flow channels can improve

the efficiency of PEMFCs. For cases with different *n*, the efficiency of cases with smaller *n* give higher efficiency for all cases with chaotic structure flow channels. Thus, smaller *n* is benefit to the efficiency of chaotic flow channel PEMFCs. However, the influence of *n* on cases with α equal to 90° (with promote ratios equal to 7.70% and 5.63% respectively) is more obvious than cases with α equal to 45° (whose promote ratios are 1.26% and 0.94%). As for the influence of α on efficiency, it varies with the value of *n*. When *n* equal to 10, the efficiencies of cases whose flow channel corner angles α equal to 90° are slightly larger than those of cases whose flow channel corner angles α equal to 45°. When it comes to compare cases under situation that *n* equal to 14, cases with the flow channel corner angles α equal to 45° perform better than the corresponding cases with the flow channel corner angles α equal to 90°. However, how will the value of α influences efficiencies of PEMFCs as the value of *n* increasing can be investigated in later researches.

5. Conclusions

The effects of different shape chaotic structure flow channels on different performances of PEMFCs are numerically investigated in this paper. Nine different chaotic flow channels including 2 flow channel datum surface numbers (*m*= 1 and 2), 2 flow channel corner angles (α= 90° and 45°) and 2 flow channel bends amount (*n*= 10 and 14) are considered. The temperature and velocity fields, temperature uniformity, output power, pressure drop and efficiency are analyzed. The main conclusions are summarized as:

(1) The temperatures of the cases whose flow channels datum surface number equal to 2 are significantly lower in the middle part of the whole PEMFC. The increase of the flow channel datum surface and the decrease of the amount of flow channel bends are propitious to enhance the uniformity of the membrane mid surface temperature. The influence of flow channel corner angles depends on whether the flow channels have only one datum surface or more.

(2) Chaotic structure is advantageous to velocity increasing effect in flow channels of PEMFCs. In cases with chaotic structure flow channels, cases with larger flow channel angles and smaller flow channel bends amount have more violent velocity increasing effect. And the influence of flow channel corner angles on the location and area of dead zone is much more obviously than the influence of flow channel bends amount. For chaotic structure cases with different flow channel datum surface number, the general velocity trend and dead zone locations are similar with each other. But larger flow channel datum surface number will lead to smaller area of high velocity region and dead zone.

(3) Chaotic structure is beneficial for the output power of the PEMFC. The effects of flow channel datum surfaces, flow channel corner angle and flow channel bends is different on the PEMFC. Increasing flow channel datum surface number are benefit to the maximum output power for PEMFCs with chaotic structure flow channels.

(4) The flow channel corner angle has quite obvious influence on the pressure drop of the anode flow channel (pressure drops of cases whose α equal to 45° are smaller than pressure drops of cases whose α equal to 90°) while the influence of flow channel datum surface number and the flow channel number (smaller m and n is, smaller the pressure drop is) on the pressure drop is much smaller.

(5) Chaotic structure flow channels are beneficial to the efficiency of PEMFCs. Increasing flow channel datum surface number and flow channel bends number can improve the efficiency of PEMFCs. As for the influence of flow channel corner angle on PEMFCs' efficiency varies with the value of flow channel bends number.

Acknowledgements

This work was sponsored by the the National Natural Science Foundation of China (51676163) and the National 111 Project under Grant no. B18041. Prof. Meng Ni would thank

the grant (Project Number: PolyU 152214/17E) from Research Grant Council, University Grants Committee, Hong Kong SAR.

References

[1] Appleby AJ. Fuel Cell Handbook. 2004.

[2] Costamagna P, Srinivasan S. Quantum jumps in the PEMFC science and technology from the 1960s to the year 2000: Part II. Engineering, technology development and application aspects. *Journal of Power Sources* 2001;102(1):242-252.

[3] Kulikovsky AA, Oetjen HF, Wannek C. A simple and accurate method for high-temperature PEM fuel cell characterization. *Fuel cells* 2010;10(3):363-368.

[4] Rau M, Niebergesab A, Cremers C, Alfaro S, Steenberg T, Hjuler HA. Characterization of membrane electrode assemblies for high-temperature. *Fuel cells* 2016;16(5):577-583.

[5] Wang XC, Zhou B, Jiang MC. Dynamic contact angle effects on gas-liquid transport phenomena in proton exchange membrane fuel cell cathode with parallel design. *International Journal of Energy Research* 2018;42:4439-4457.

[6] Kuo JK, Li HY, Weng WC, Yan WM. Numerical investigation into transient response of proton exchange membrane fuel cell with serpentine flow field. *International Journal of Energy Research* 2013;37(11):1302-1312.

[7] Ibrahimoglu B, Yilmazoglu MZ, Celenk S. Investigation of spiral flow-field design on the performance of a PEM fuel cell. *Fuel Cells* 2017;17(6):786-793.

[8] Schepper PD, Danilov VA, Denayer JFM. Cathode flow field design for nitric oxide/hydrogen fuel cell in cogeneration of hydroxylamine and electricity. *International Journal of Energy Research* 2016;40:1355-1366.

[9] Wen DH, Yin LZ, Piao ZY, Lu CD, Li G, Leng QH. A novel intersectant flow field of metal bipolar for proton exchange membrane fuel cell. *International Journal of Energy Research* 2017;41:2184-2193.

[10] Chen T, Liu S, Gong S, Wu C. Development of bipolar plates with different flow channel configurations based on plant vein for fuel cell. *International Journal of Energy Research* 2013;37(13):1680-1688.

[11] Ahmidi N, Dadvand A, Mirzaei I, Rezazadeh S. Modeling of polymer electrolyte membrane fuel cell with circular and elliptical cross-section gas channels: A novel procedure. *International Journal of Energy Research* 2018;42(8):2805-2822.

[11] Yin Y, Wang XF, Shangguan X, Zhang JF, Qin YZ. Numerical investigation on the characteristic of mass transport and performance of PEMFC with baffle plates installed in the flow channel *International Journal of Hydrogen Energy* 2018;43:8048-8062.

[12] Shen J, Tu ZK, Chan SH. Enchantment of mass transfer in a proton exchange membrane fuel cell with blockage in the flow channel. *Applied Thermal Engineering* 2019;149:1408-1418.

[13] Khan SS, Shareef H, Wahyudie A, Khalid SH. Novel dynamic semi empirical proton exchange membrane fuel cell model incorporating component voltages. *International Journal of Energy Research* 2018;42(8): 2615-2630.

[14] Ye Dh, Tu ZK, Yu Y, Cai YH, Zhang HN, Zhan ZG, Pan M. Hydrogen permeation across super-thin membrane and the burning limitation in low-temperature proton exchange membrane fuel cell. *International Journal of Energy Research* 2014;38:1181-1191.

[15] Qin YZ, Yin Y, Jiao K, Du Q. Effect of needle orientation and gas velocity on water transport and removal in a modified PEMFC gas flow channel having a hydrophilic needle. *International Journal of Energy Research* 2018;1-12.

[16] Yin Y, Wang XF, Zhang JF, Shangguan X, Qin YZ. Influence of sloping baffle plate on the mass transport and performance of PEMFC. *International Journal of Energy Research* 2018;1-13.

[17] Chen B, Wang J, Yang TQ, Cai YH, Pan M, Tu ZK, Zhang CZ, Chan SH, Yu Y. Mitigation studies of carbon corrosion by optimizing the opening size of the cathode outlet in a proton exchange membrane fuel cell with dead-ended anode. *Energy Conversion and Management* 2016;119:60-66.

[18] Chen H, Guo H, Ye F, Ma CF, Liao Q, Zhu X. Mass transfer in proton exchange membrane fuel cells with baffled flow channels and a porous-blocked baffled flow channel design. *International Journal of Energy Research* 2019;1-20.

[19] Cai YH, Fang Z, Chen B, Yang TQ, Tu ZK. Numerical study on a novel 3D cathode flow field and evaluation criteria for the PEM fuel cell design. *Energy* 2018;161:28-37.

[20] Mokrani A, Castelain C, Peerhossaini H. The effects of chaotic advection on heat transfer. *International Journal of Heat and Mass Transfer* 1997;40(13):3089-3104.

[21] Lefevre A, Mota JPB, Rodrigo AJS, Saatdjian E. *Chaotic advection and heat transfer enhancement in stokes flows* 2003;24(3):310-321.

[22] Bahiraei M, Mazaheri N. Application of a novel hybrid nanofluid containing graphene-platinum nanoparticles in a chaotic twisted geometry for utilization in miniature devices: Thermal and energy efficiency considerations. *International Journal of Mechanical Sciences* 2018;138-139:337-349.

[23] Bahiraei M, Mazaheri N, Alighardashi M. Development of chaotic advection in laminar flow of a non-Newtonian nanofluid: A novel application for efficient use of energy. *Applied Thermal Engineering* 2017;124:1213-1223.

[24] Bahiraei M, Hangi M. Numerical investigation and optimization of flow and thermal characteristics of nanofluid within a chaotic geometry. *Advanced Powder Technology* 2016;27:184-192.

[25] Lemenand T, Peerhossaini H. A thermal model for prediction of the Nusselt number in a pipe with chaotic flow. *Applied Thermal Engineering* 2002;22(15):1717-1730.

[26] Acharya N, Sen M, Chang HC. Analysis of heat transfer enhancement in coiled-tube heat exchangers. *International Journal of Heat and Mass Transfer* 2001;44(17):3189-3199.

[27] Castelain C, Lasbet Y, Auvity B, Peerhossaini H. Experimental study of the thermal performance of chaotic geometries for their use in PEM fuel cells. *International Journal of Thermal Sciences* 2016;101:181-192.

[28] Xuan J, Leung DYC, Leung MKH, Wang H, Ni M. Chaotic flow-based fuel cell built on counter-flow microfluidic network: predicting the over-limiting current behavior. *Journal of Power Sources* 2011;196(22):9391-9397.

[29] Kuo JK, Huang PH, Wang CF. Numerical modeling and analysis of PEMFC integrated with auxiliary power source. *International Journal of Energy Research* 2013;37:1635-1644.

[30] Carcadea E, Varlam M, Ingham DB, Ismail MS, Patularu L, Marinoiu A, Schitea D. The effects of cathode flow channel size and operating conditions on PEM fuel performance: A CFD modelling study and experimental demonstration. *International Journal of Energy Research* 2018;42:2789-2804.

[31] Bilgili M, Bosomoiu M, Tsotridis G. Gas flow field with obstacles for PEMFCs at different operations. *International Journal of Hydrogen Energy* 2014;40(5):2303-2311.

[32] Akbari MH, Rismanchi B. Numerical investigation of flow field configuration and contact resistance for PEMFC performance. *Renewable Energy* 2008;33(8):1775-1783.

[33] Kuo JK, Yen TH, Chen CK. Three-dimensional numerical analysis of PEMFCs with straight and wave-like gas flow fields channels. *Journal of Power Sources* 2008;177(1):96-103.

[34] Fontana E, Mancusi E, Silva AD, Mariani VC, Souza AAUD, Souza SMAGUD. Study of the effects of flow channel with non-uniform cross-sectional area on PEMFC species and heat transfer. *International Journal of Heat and Mass Transfer* 2011;54(21):4462-4472.

[35] Guvelioglu GH, Stenger HG. Computational fluid dynamics modeling of polymer electrolyte membrane fuel cells. *Journal of Power Sources* 2005;147(1-2):95-106.

[36] Scholta J, Escher G, Zhang W, Kuppers L, Jorissen L, Lehnert W. Investigation on the influence of channel geometries on PEMFC performance. *Journal of Power Sources* 2006;155(1):66-71.

[37] Yang WJ, Kang SJ, Kim YB. Numerical investigation on the performance of proton exchange membrane fuel cells with channel positon variation. *International Journal of Energy Research* 2012;36:1051-1064.

[38] Barbir, Frano. PEMFC: theory and practice, 2nd edition. Elsevier Academic Press 2013.

[39] Wang L, Husar A, Zhou TH, Liu HT. A parametric study of PEMFC performance. *International Journal of Hydrogen* 2003; 28:1263-1272.

Figure and Table Captions

Figure 1 Schematic diagram of PEMFC with serpentine flow channels. (a) A sketch of 3D integrated system; (b) Geometrical descriptions of Hydrogen inlet and membrane electrode assembly; (c) Representative line and surfaces for the paper analysis.

Figure 2 Sketch of ten serpentine flow channels (Case A1: straight; Cases A2 and B-E: Chaotic) and indication of main design parameters (take Case E2 as an example).

Figure 3 Unstructured grids near the flow channels in used the presented simulations (take Case E1 as an example).

Figure 4 Stream-wise velocity comparison along centerline of anode flow channel (Line 1 in Fig.1 (c)) under different mesh sizes. Case A1, u_{an}= 1200 *sccm*, u_{ca}= 2200 *sccm*.

Figure 5 Comparison of the simulated results with available experimental data in terms of polarization curves (Wang et al. [39]). u_{an}= 1200 *sccm*, u_{ca}= 2200 *sccm*.

Figure 6 Temperature distribution on mid surface in z axis direction of membrane (Sur 1 in Fig. 1 (c), z= 0 *mm*). u_{an}= 1200 *sccm*, u_{ca}= 2200 *sccm*.

Figure 7 Uniformity of temperature on mid surface in z axis direction of membrane (Sur 1 in Fig. 1 (c), z= 0 *mm*). (a) Mean deviation; (b)Standard deviation.

Figure 8 Velocity distribution on anode flow channel mid surface in z axis (Sur 2 and Sur 3 for cases 1 and 2, respectively). u_{an}= 1200 *sccm*, u_{ca}= 2200 *sccm*.

Figure 9 Flow streamlines in streamwise-normal planes (Sur 4, Sur 5 and Sur 6 in Fig. 1 (c)) at u_{an}= 1200 *sccm*, u_{ca}= 2200 *sccm* for cases with different flow channel datum surface numbers (first to forth rows: cases A1, A2, B1 and B2).

Figure 10 Flow streamlines of cases with different flow channel bends numbers and angles in streamwise-normal planes.u_{an}= 1200 *sccm*, u_{ca}= 2200 *sccm*. (first to fifth rows: Cases A1, B1, C1, D1 and E1).

Figure 11 Comparison of current-power curves with different flow channel datum surface numbers ((a) and (b)), bends numbers ((c) and (d)) or bends angles ((e) and (f)). (a) Cases A1 and A2; (b) Cases B1 and B2; (c) Cases A1, B1 and D1; (d) Cases A2, B2 and D2; (e) Cases A1, B1 and C1; (f) Cases A1, D1 and E1.

Figure 12 A comparison between maximum output powers of all ten cases in this research. u_{an}= 1200 *sccm*, u_{ca}= 2200 *sccm*.

Figure 13 Inlet-to-outlet pressure drops on anode flow channel mid surface (Sur 2 and Sur 3 for cases 1 and 2 respectively as shown in Fig. 1 (c)). u_{an}= 1200 *sccm*, u_{ca}= 2200 *sccm*.

Figure 14 The value of net efficiencies of cases with nine chaotic structures flow channels (cases A2, B-E) and straight flow channel (Case A1) as reference.

Table 1 Parameters of computational domain, flow channels and single PEMFC used in process of model developing.

Table 2 Main geometry parameters of chaotic structure flow channels in all ten cases including one case with straight flow channel (Case A1) and nine cases with chaotic structure flow channels (cases A2, B-E).

Table 3 Details of key operating parameters used in numerical simulations.

Table 1 Parameters of computational domain, flow channels and single PEMFC used in process of model developing.

Parameters		Value (mm)
Parameters of computational domain	W_{cd}	14
	L_{cd}	18
	H_{cd}	4.55
Parameters of flow channels	W_{ch}	2
	W_{in}	2
	H_{ch}	1
	H_r	0.5
	L_{ch}	16
	W_{d1}	6
	W_{d2}	8
	L_d	10
Parameters of single PEMFC	H_p	2
	H_{dl}	0.05
	H_{pem}	0.05
	H_{cl}	0.2

Table 2 Main geometry parameters of chaotic structure flow channels in all ten cases including one case with straight flow channel (Case A1) and nine cases with chaotic structure flow channels (cases A2, B-E).

Cases	α (°)	n (mm)	m (mm)
A1	/	4	
B1	90	10	
C1	45	10	1
D1	90	14	
E1	45	14	
A2	/	4	
B2	90	10	
C2	45	10	2
D2	90	14	
E2	45	14	

Table 3 Details of key operating parameters used in numerical simulations.

Parameters	Units	Value
Stoichiometry in anode		1.5
Stoichiometry in cathode		3
Porosity of diffusion layer		0.5
Porosity of catalytic layer		0.6
Conductivity coefficient of PEM		1
Conductivity index of PEM		1
Heat transfer coefficient of PEM	$W \cdot m^{-1} \cdot K^{-1}$	0.95
Conductivity of PEM	$\Omega^{-1} \cdot m^{-1}$	12.99
Ratio of catalytic layer surface area to volume	m^{-1}	2×10^5
Viscous resistance of diffusion layer/catalytic layer	m^{-2}	5×10^{12}
Reference exchange current density in anode	$A \cdot m^{-2}$	1×10^9
Reference exchange current density in cathode	$A \cdot m^{-2}$	1×10^4
Reference molar concentration in anode	$kmol \cdot m^{-3}$	44.4
Reference molar concentration in cathode	$kmol \cdot m^{-3}$	44.4
Current density	$A \cdot m^{-2}$	1
Open circuit voltage	V	0.95
Operating temperature	K	353

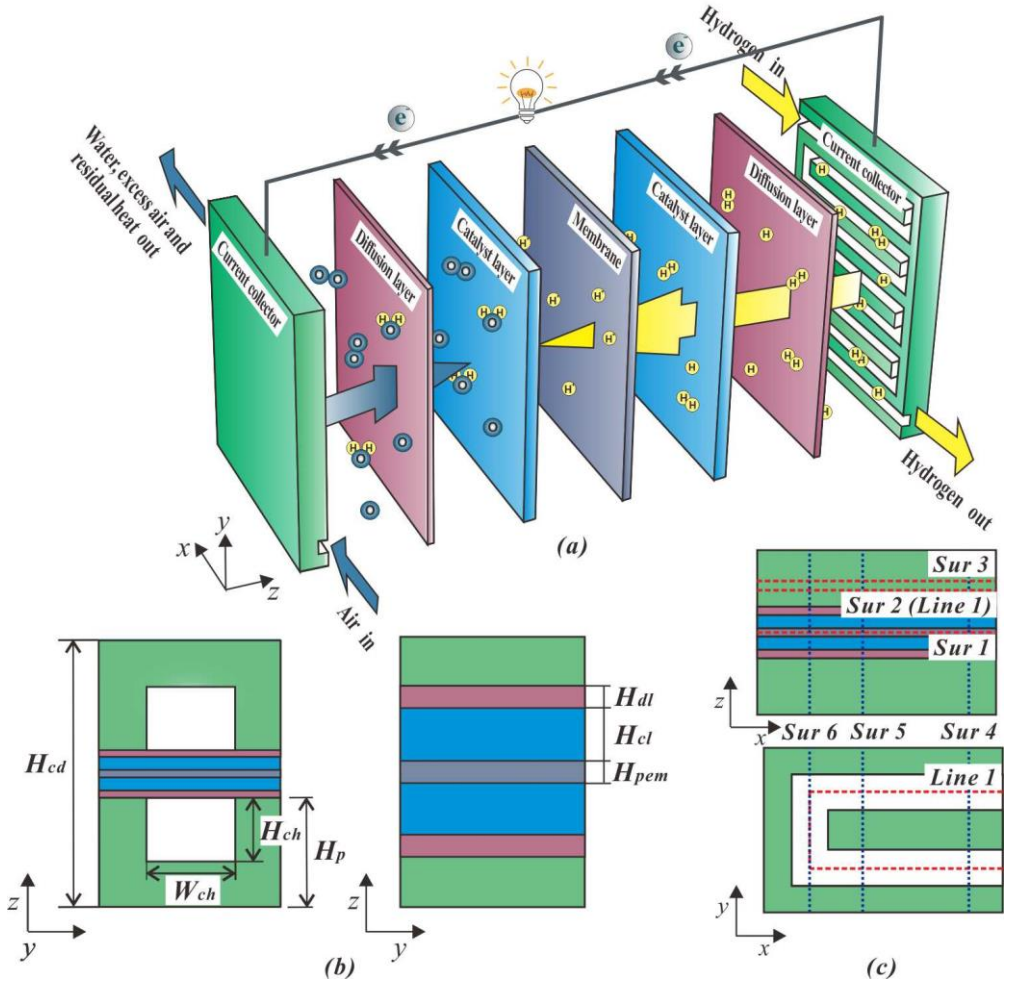

Fig. 1 Schematic diagram of PEMFC with serpentine flow channels. (a) A sketch of 3D integrated system; (b) Geometrical descriptions of Hydrogen inlet and membrane electrode assembly; (c) Representative line and surfaces for the paper analysis.

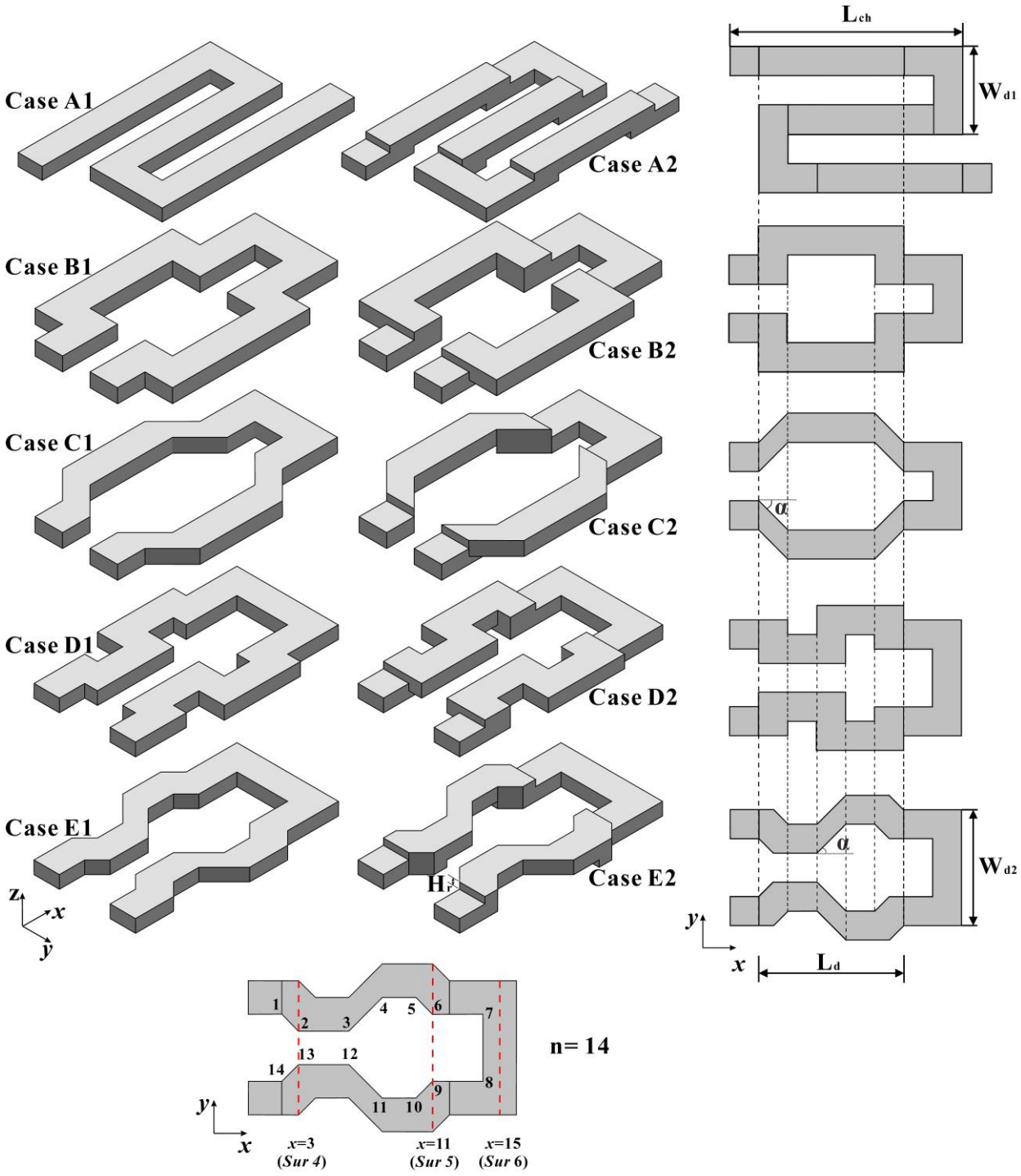

Fig.2 Sketch of ten serpentine flow channels (Case A1: straight; Cases A2 and B-E: Chaotic) and indication of main design parameters (take Case E2 as an example).

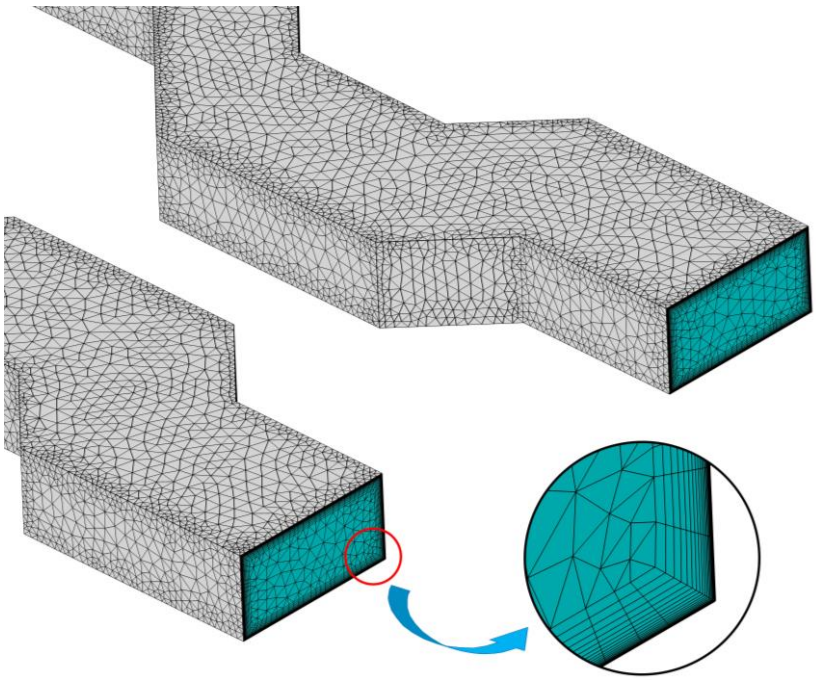

Fig.3 Unstructured grids near the flow channels in used the presented simulations (take Case E1 as an example)

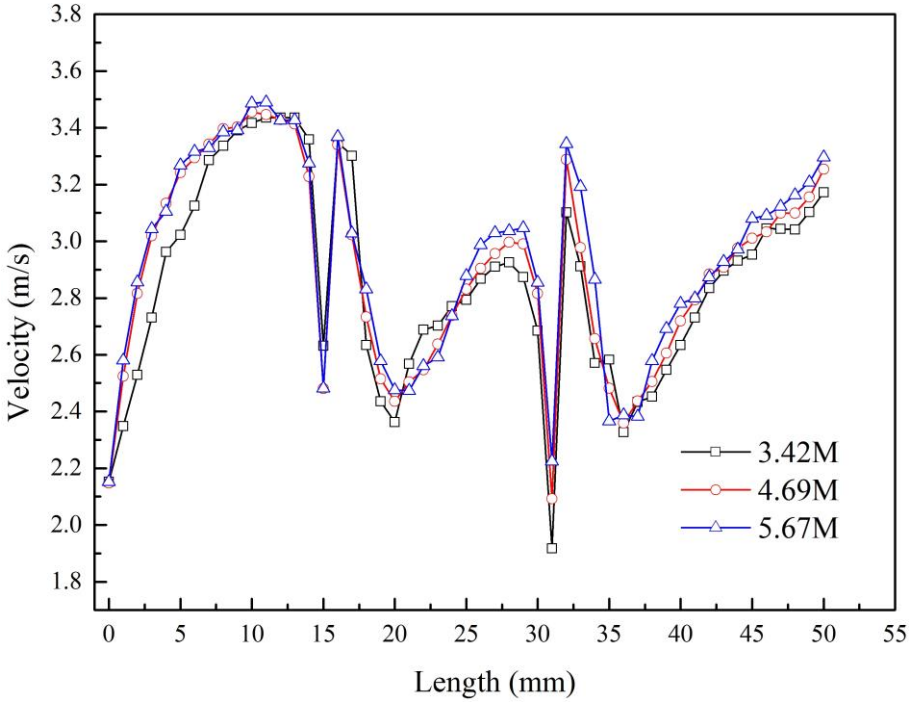

Fig.4 Stream-wise velocity comparison along centerline of anode flow channel (Line 1 in Fig.1 (c)) under different mesh sizes. Case A1, u_{an}= 1200 *sccm*, u_{ca}= 2200 *sccm*.

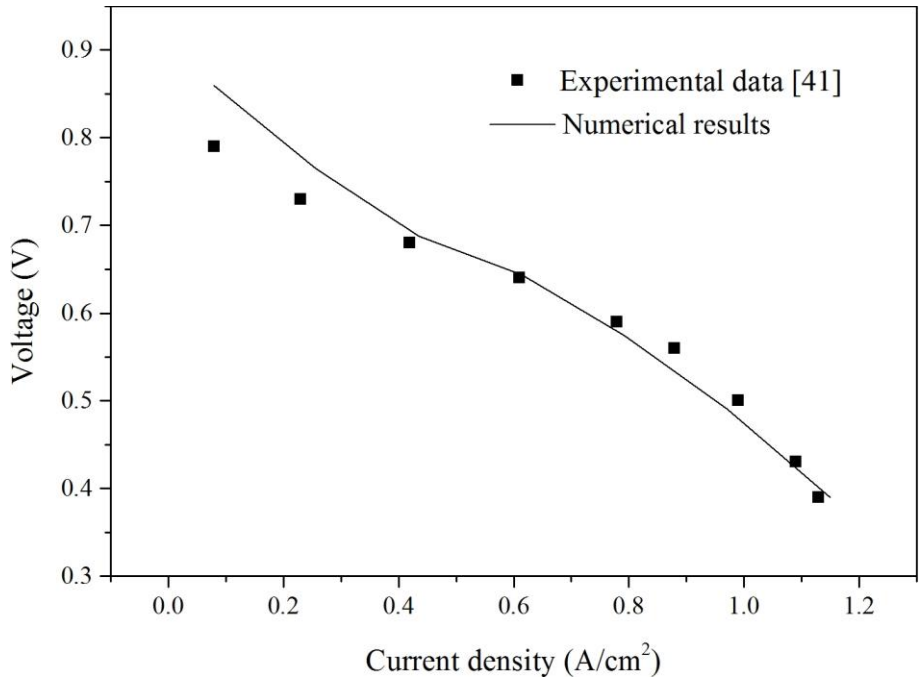

Fig. 5 Comparison of the simulated results with available experimental data in terms of polarization curves (Wang et al. [39]). u_{an}= 1200 *sccm*, u_{ca}= 2200 *sccm*.

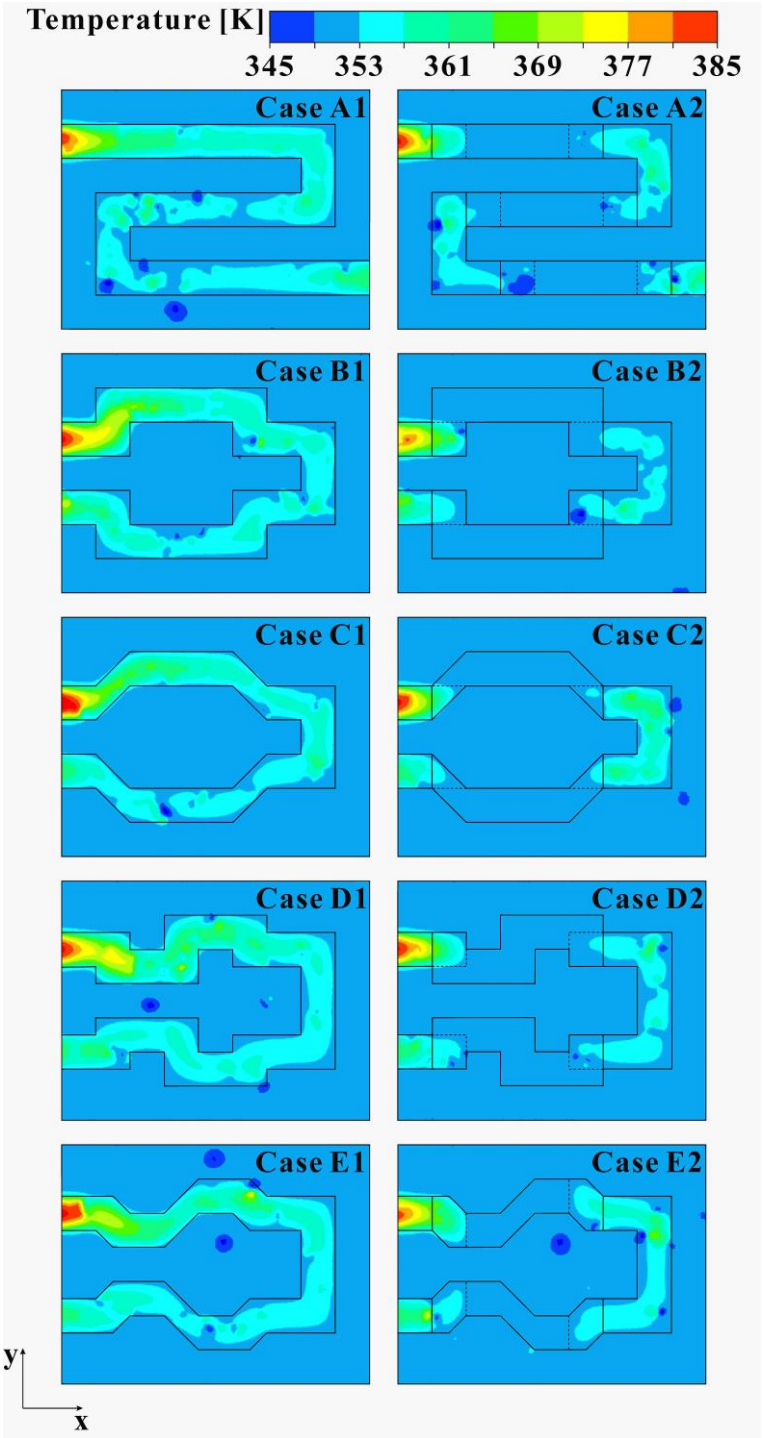

Fig. 6 Temperature distribution on mid surface in z axis direction of membrane (Sur 1 in Fig. 1 (c), *z*= 0 *mm*). u_{an}= 1200 *sccm*, u_{ca}= 2200 *sccm*.

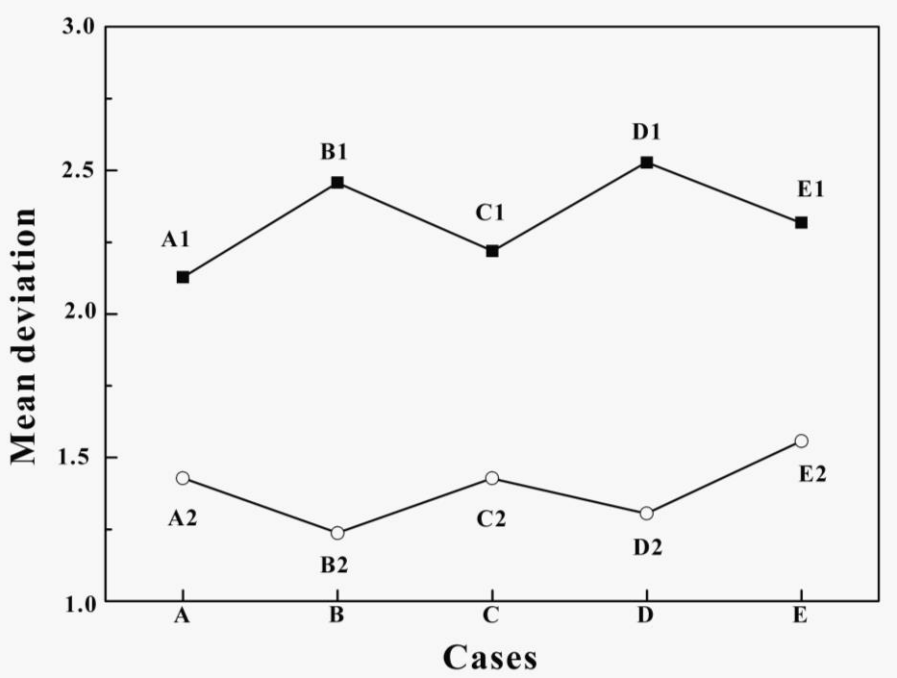

(a)

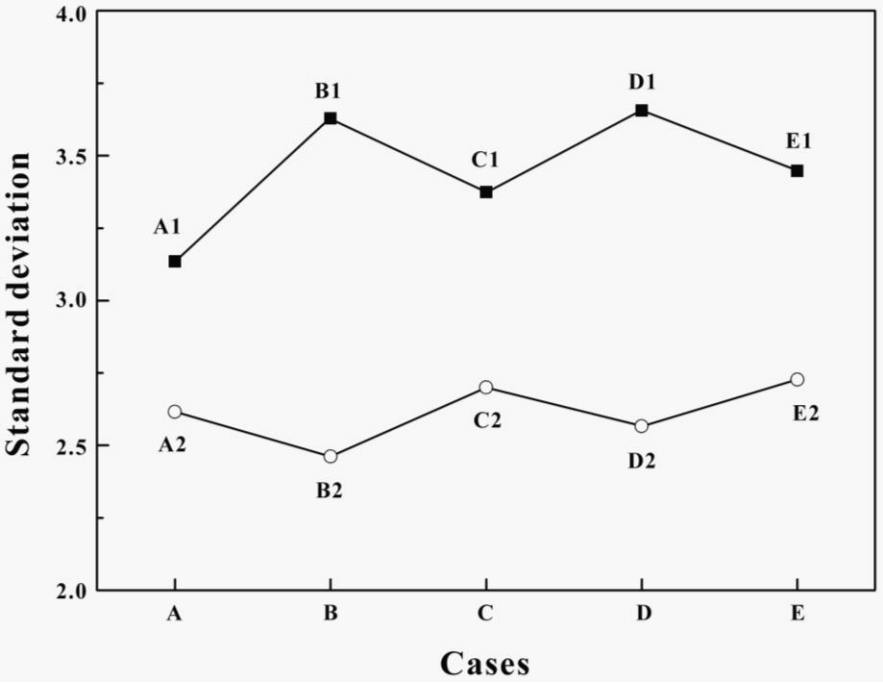

(b)

Fig. 7 Uniformity of temperature on mid surface in z axis direction of membrane (Sur 1 in Fig. 1 (c), *z*= 0 *mm*). (a) Mean deviation; (b)Standard deviation.

/

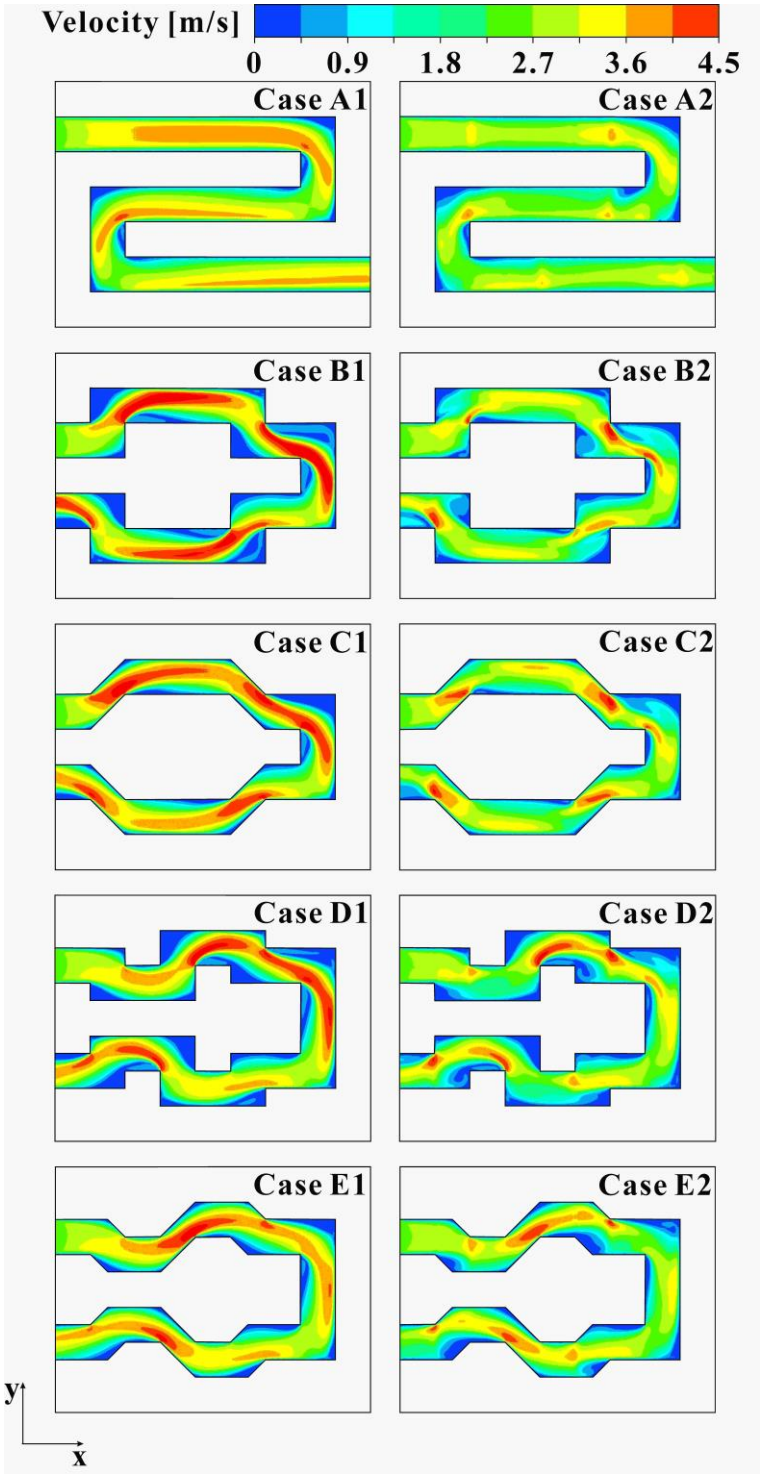

Fig. 8 Velocity distribution on anode flow channel mid surface in z axis (Sur 2 and Sur 3 for cases 1 and 2, respectively). u_{an}= 1200 *sccm*, u_{ca}= 2200 *sccm*.

/

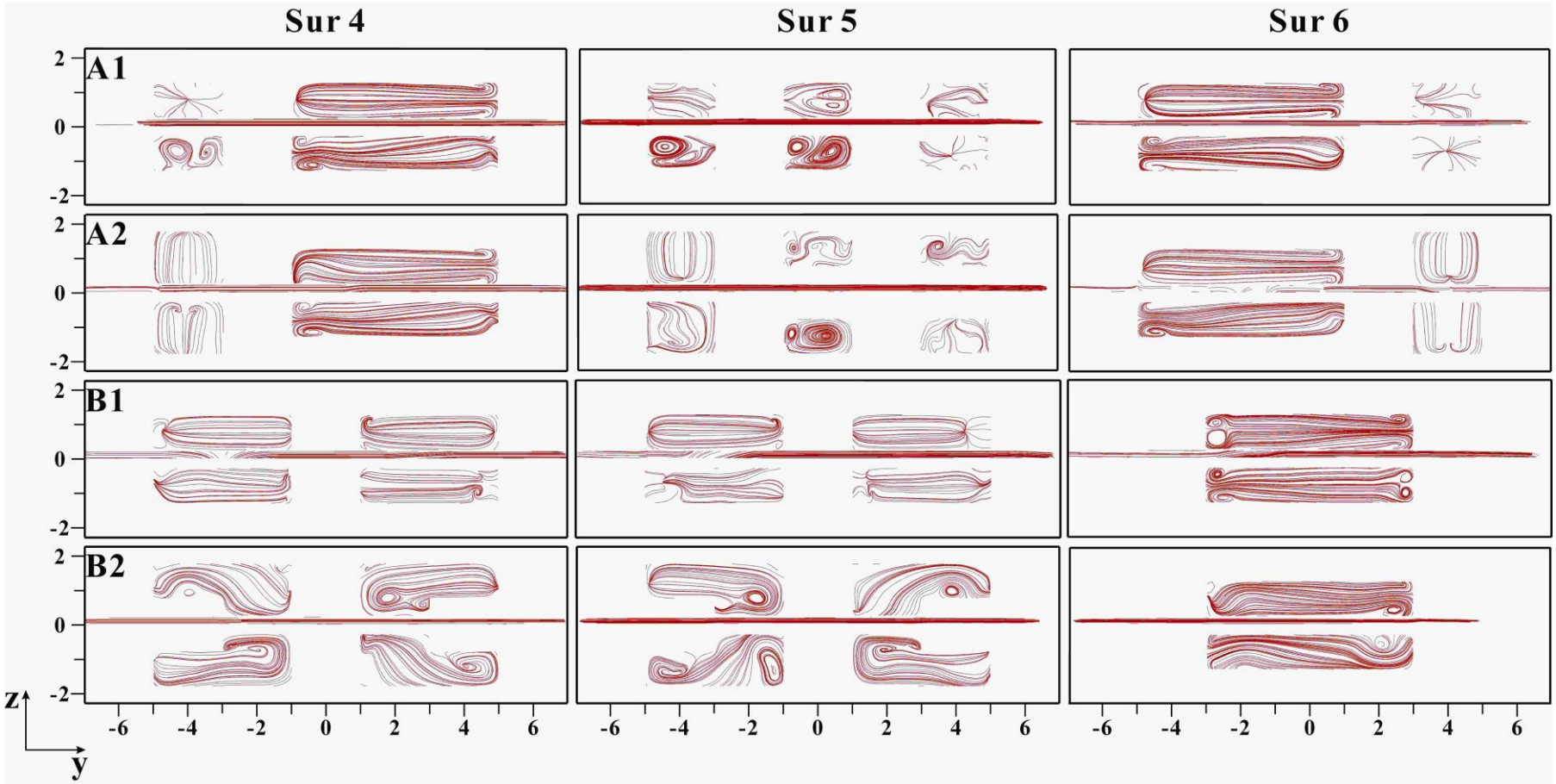

Fig. 9 Flow streamlines in streamwise-normal planes (Sur 4, Sur 5 and Sur 6 in Fig. 1 (c)) at u_{an}= 1200 *sccm*, u_{ca}= 2200 *sccm* for cases with different flow channel datum surface numbers (first to forth rows: cases A1, A2, B1 and B2).

/

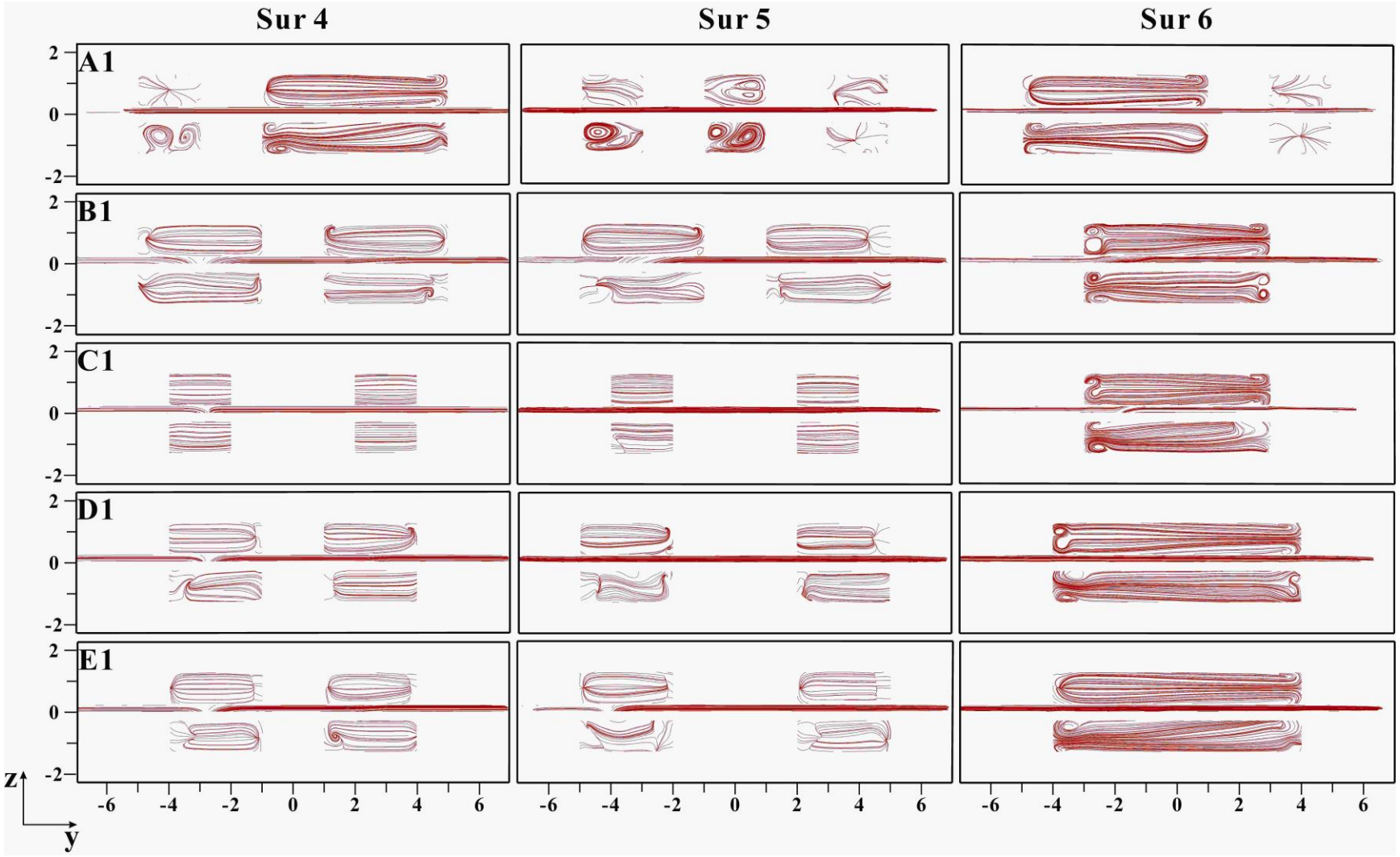

Fig. 10 Flow streamlines of cases with different flow channel bends numbers and angles in streamwise-normal planes. u_{an}= 1200 *sccm*, u_{ca}= 2200. (first to fifth rows: cases A1, B1, C1, D1 and E1).

/

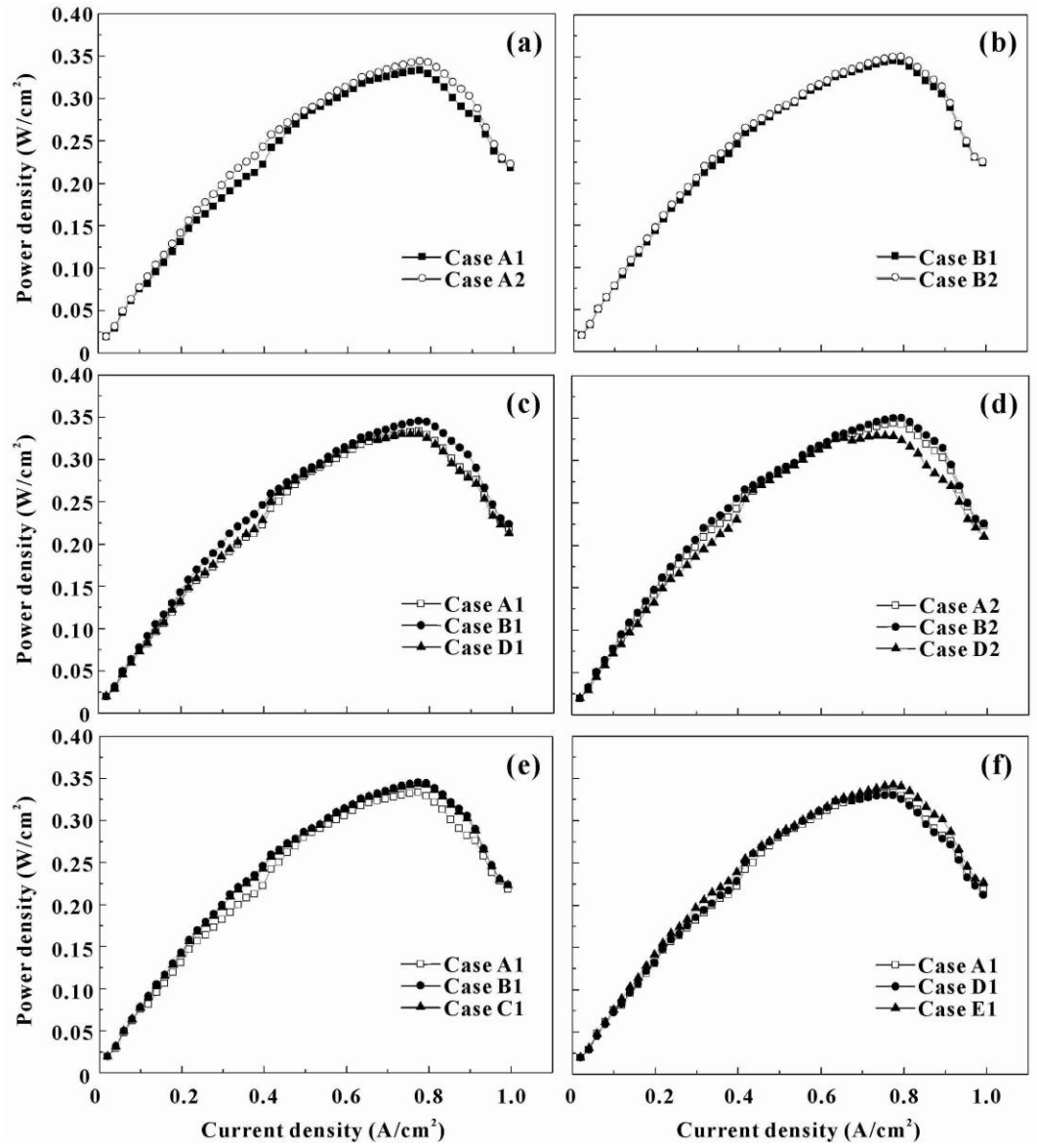

Fig.11 Comparison of current-power curves with different flow channel datum surface numbers ((a) and (b)), bends numbers ((c) and (d)) or bends angles ((e) and (f)). (a) Cases A1 and A2; (b) Cases B1 and B2; (c) Cases A1, B1 and D1; (d) Cases A2, B2 and D2; (e) Cases A1, B1 and C1; (f) Cases A1, D1 and E1.

/

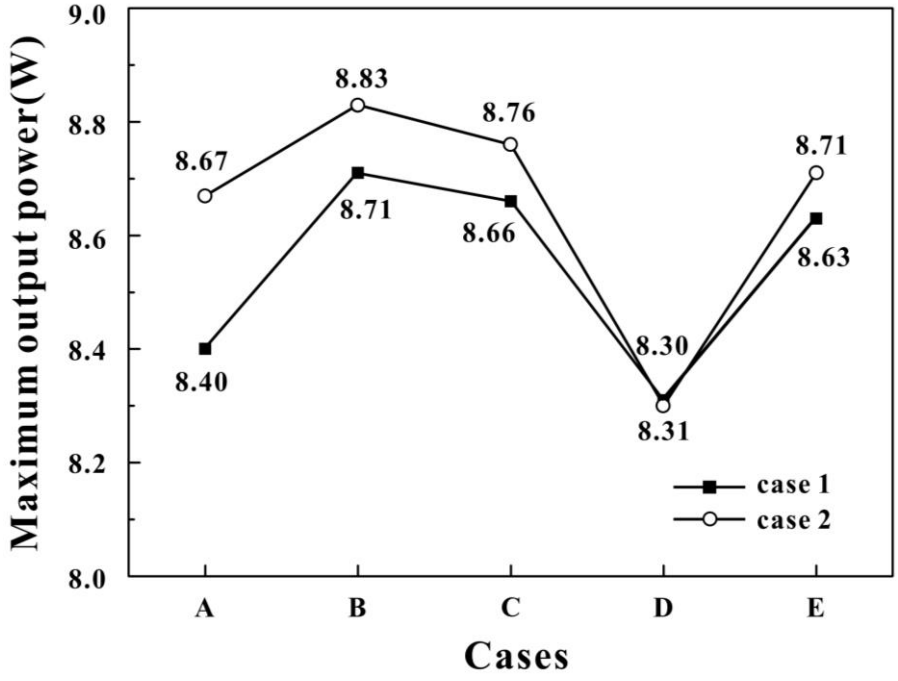

Fig. 12 A comparison between maximum output powers of all ten cases in this research. u_{an}= 1200 *sccm*, u_{ca}= 2200 *sccm*.

/

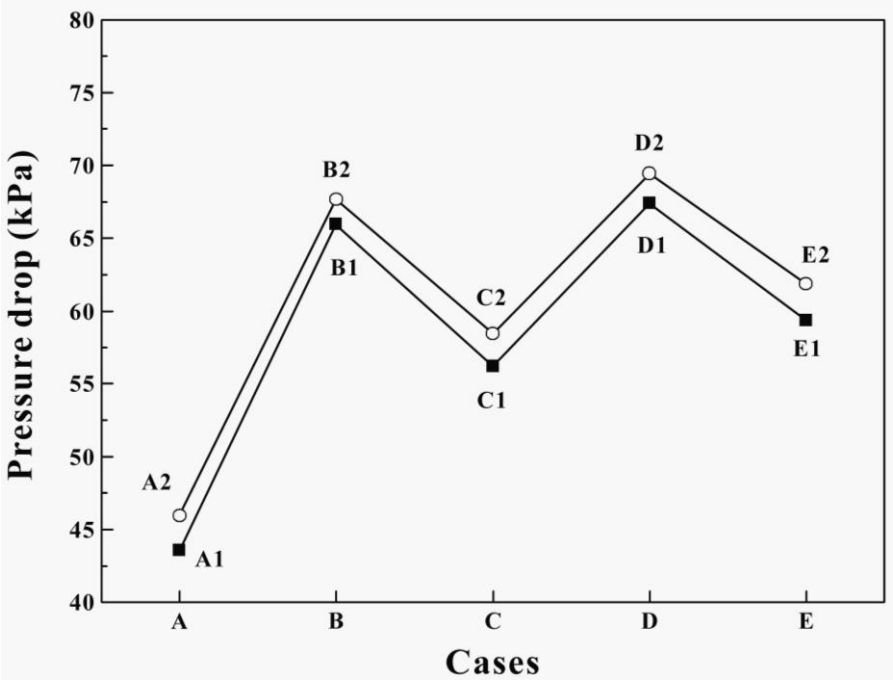

Fig. 13 Inlet-to-outlet pressure drops on anode flow channel mid surface (Sur 2 and Sur 3 for cases 1 and 2 respectively as shown in Fig. 1 (c)). u_{an}= 1200 *sccm*, u_{ca}= 2200 *sccm*.

/

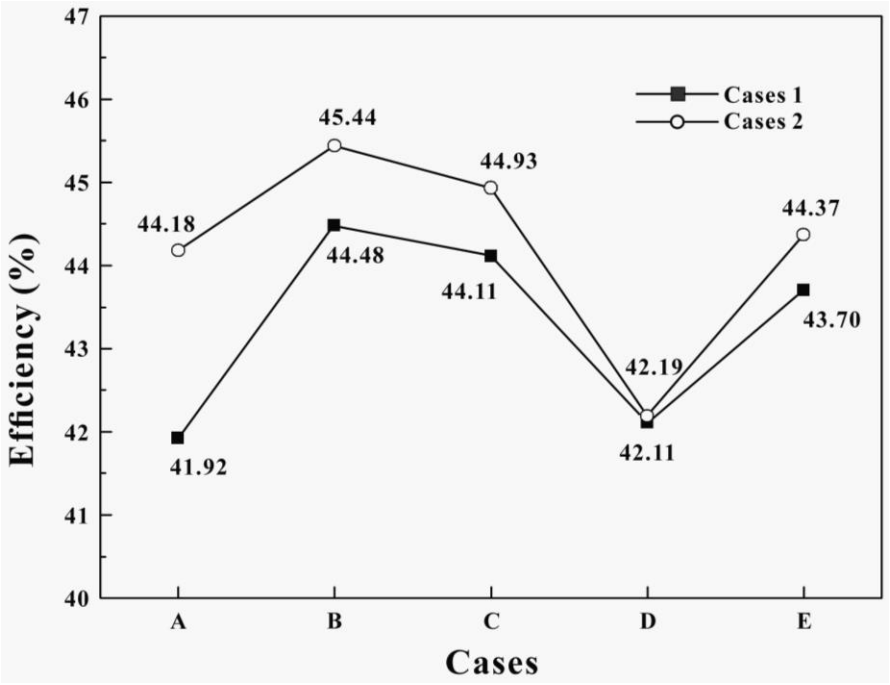

Fig. 14 Comparison of PEMFCs' efficiencies.

/